Measurements of velocity and concentration in a high Reynolds number turbulent boundary layer

Krishna M. Talluru

School of Civil Engineering
The University of Sydney
NSW 2006 AUSTRALIA
murali.talluru@sydney.edu.au

Chiala Hernandez-Silva

School of Civil Engineering
The University of Sydney
NSW 2006 AUSTRALIA
cher6753@uni.sydney.edu.au

Jimmy Philip

Dept. of Mechanical Engineering
The University of Melbourne
VIC 3010 AUSTRALIA
jimmyp@unimelb.edu.au

Kapil A. Chauhan

School of Civil Engineering
The University of Sydney
NSW 2006 AUSTRALIA
kapil.chauhan@sydney.edu.au

ABSTRACT

Measurements of velocity and concentration fluctuations for a horizontal plume released at eight different heights within a turbulent boundary layer (TBL) are discussed in this paper. Most previous studies have reported measurements for the source height limited to $s_z/\delta \leq 0.2$ (s_z is the source height and δ is the boundary layer thickness). Here we examine concentration fluctuations when the plume is released in the logarithmic and outer regions of a TBL in order to understand the role of large-scale structures in the transport of scalar quantities. The wall-normal distributions of mean and variance of concentration fit well with the reflected-Gaussian model as previously reported by Fackrell & Robins (1982). A comparison of autocorrelation functions reveals that the integral time scale of the corresponding concentration fluctuations is approximately ten times smaller than the integral time scale of streamwise velocity. Further, it is observed that streamwise scalar flux and cross-correlation coefficient between large-scale velocity and concentration have similar behaviour, i.e., they are positively correlated below and negatively correlated above the plume centreline.

1 INTRODUCTION

Urbanisation has led to an increase in number of pollutant sources, both ground and elevated. This effects the urban air quality, and thus it is important to estimate the spread of contaminant in the atmosphere due to sources at varying heights. Previous studies (e.g. Fackrell & Robins, 1982; Gailis & Hill, 2006; Nironi *et al.*, 2015) have documented the behaviour of mean concentration profiles for a ground level and an elevated source. Fackrell & Robins (1982) showed that the mean concentration for a ground level plume has an exponential behaviour of the form $C = C_o \exp[-0.693(z/\delta_z)^n]$ where n is a parameter that depends on the surface roughness, z is the vertical coordinate and δ_z is the half-plume width. On the other hand, the mean concentration profile for an elevated source has a reflected-Gaussian behaviour (cf. equation 1 to be discussed in a later section in this paper).

The concentration fluctuations are of great interest, since mean concentration distribution provides little information about the peak values of concentration and the associated hazard which may occur over short duration and in small volumes. Direct measurements of fluctuating concentration levels in the atmosphere are difficult to obtain due to non-stationary conditions, limitations of instrumentation and the physical scale of atmospheric flows. In this regard, Yee *et al.* (1993) emphasised the need for wind tunnel facilities to simulate the large-scales that are responsible for plume meandering. Metzger & Klewicki (2003) employed photo-ionisation technique to improve the frequency response of concentration sensors to record instantaneous fluctuations of concentration and experimentally evaluate scalar fluxes. A similar photo-ionisation detector (PID) is used for measuring concentration in the current study.

Concurrently, there have been advancements in understanding the structure of a TBL. Particularly, the role of large-scale structures in transporting momentum and modulating fine-scale turbulence close to the surface (Smits *et al.*, 2011; Hutchins & Marusic, 2007*a*,*b*; Marusic *et al.*, 2010, and references therein) is now well understood. It is known that lateral ($\overline{vc}$) and vertical ($\overline{wc}$) scalar fluxes (where v and w are the velocity fluctuations in the lateral and vertical directions respectively and c is the concentration fluctuation) contribute to the spread of plume. Extending the work of Hutchins & Marusic (2007*b*), Talluru *et al.* (2014*a*) showed that large-scale streamwise velocity structures modulate the three components of velocity fluctuations and also the Reynolds shear stresses, which in the context of plume dispersion will contribute to the spread of plume. These recent findings necessitate investigation to link these results to scalar dispersion and quantify the interaction between a plume and the so-called 'canonical' TBL. As a first step towards understanding this interaction, here we aim to characterise the cross-correlation between large-scale fluctuations of velocity and concentration.

2 EXPERIMENTAL SETUP

Experiments are conducted in the closed-circuit Boundary Layer Wind Tunnel (BLWT) at the University of Sydney. The wind tunnel has a long working section of 19 m and has a cross-section of 2.5 m wide $\times$ 2.0 m height. The roof height is constant in the region, $0 \leq x \leq 12$ m leading to a mild favourable pressure gradient equivalent to 3% increase in the free stream velocity over that distance. Note that x is the streamwise distance measured from the trip, a 50 mm wide SP60 grit sandpaper spanning the full width of the tunnel to trigger transition to turbulence of the incoming laminar boundary layer. Between $x = 12$ m and $x = 17$ m, the roof is made of horizontal slats that are adjusted to achieve nominally zero pressure gradient in the region $12\,\text{m} \leq x \leq 17\,\text{m}$. The flow is driven by a 250 kW fan and the flow passes through several flow conditioning elements before entering the contraction with an area ratio of

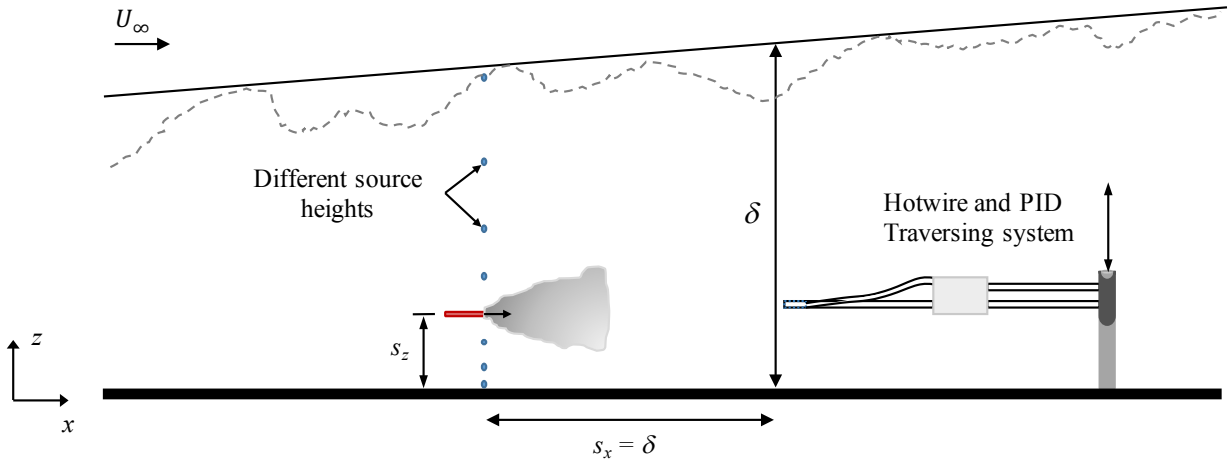

Figure 1: Schematic of experimental setup.

Source heights:	
s_z/δ = 32/δ^+, 350/δ^+, 0.1, 0.25, 0.33, 0.5 , 0.67, δ_{99}/δ.	
Boundary layer properties at x = 13 m:	
$l^+ \approx 24$,	$d^+_{\mathrm{PID}} \approx 18$
$\delta^+ \approx 7\,850$	$Re_\theta = 14\,300$
$U_\infty = 10.2$ m/s	$U_\tau = 0.367$ m/s
$s^+_d \approx 38$	$\delta = 0.310$ m
Tracer Gas (1.5% C_4H_8 + 98.5% N_2)	
$\rho_{\mathrm{air}} = 1.2$ kg/m^3	$\rho_{\mathrm{gas}} = 1.19$ kg/m^3
$D = 9.9\times10^{-6}$ m^2/s	$Sc = 1.52$

Table 1: Experimental parameters. (+) represents normalisation using viscous length scale, for instance, $l^+ = lU_\tau/\nu$. Here $Re_\theta = \frac{\theta U_\infty}{\nu}$, where θ is the momentum thickness. D represents the molecular diffusivity of tracer gas.

4.5:1 and then the test section. The fan is capable of generating free stream velocity (U_∞) in the range of 0 - 27 m/s and the turbulence intensity in the free stream is found to be nominally 0.5%. For the current study, U_∞ is set to 10 m/s, which resulted in a boundary layer thickness, $\delta = 0.31$ m (determined from a fit to the composite profile of Chauhan *et al.*, 2009) and friction velocity, U_τ =0.37 m/s at the measurement location, $x = 13$ m. This yields a friction Reynolds number, $Re_\tau = \delta^+ = \delta U_\tau/\nu \approx 7850$ (ν is the kinematic viscosity of air) at the measurement location.

Simultaneous measurements of velocity and concentration are made using a single hotwire and a photo-ionisation detector (PID) respectively. A schematic of the experimental setup is shown in figure 1, where various parameters are identified. The hotwire and PID sensors are mounted on a vertical traversing system at a spanwise separation of 3 mm $\approx 4d_{\mathrm{PID}}$, where $d_{\mathrm{PID}} = 0.76$ mm is the inner diameter of PID inlet tube. Both hotwire and PID are calibrated before and after each experiment and their voltage drifts during the experiment are corrected based on the calibration procedure of Talluru *et al.* (2014*b*). A point source tracer gas (a mixture of 1.5% isobutylene and 98.5% Nitrogen) is released at eight different source heights (s_z, see table 1) in the boundary layer at a streamwise separation, $s_x/\delta = 1$, upstream of the measurement location. The tracer gas is released iso-kinetically by matching the exit velocity (U_s) with the local mean velocity of the boundary layer at the source height, i.e., $U_s = U|_{(z=s_z)}$. Further details of the experimental setup and calibration procedure of PID are given in Talluru *et al.* (2017).

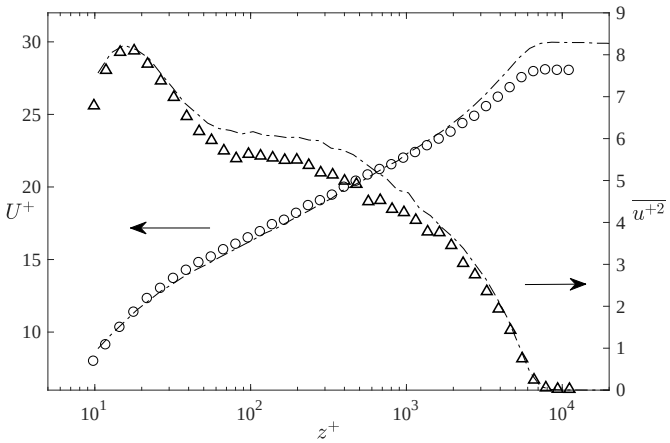

Figure 2: Comparison of mean velocity (○) and turbulence intensity (△) profiles in the current study against comparable zero-pressure gradient TBL data ($Re_\tau \approx 8\,500$) of Marusic *et al.* (2015).

2.1 Mean velocity and turbulence intensity

The inner-normalised mean velocity and turbulence intensity profiles (shown in figure 2) in the current study are compared against comparable Reynolds number ($Re_\tau = 8,500$) data of Marusic *et al.* (2015) in a smooth wall zero-pressure gradient TBL. The small differences between the two profiles are due to the mild streamwise favourable pressure gradient (FPG) in the initial fetch of the tunnel as discussed before. The results in figure 2 are consistent with the observations of Harun *et al.* (2013), who compared a favourable, zero- and adverse pressure gradient TBLs. They reported that a FPG TBL has a smaller wake component and less energetic outer region in comparison to the ZPG case; this is also seen in our current measurements.

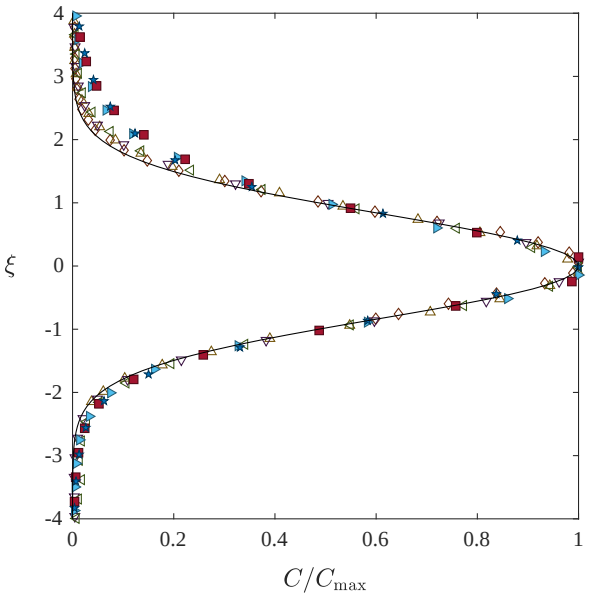

Figure 3: Normalised mean concentration ($C/C_{\max}$) profiles for different source heights indicated by symbols. Solid line is based on the reflected-Gaussian model.

2.2 Mean and r.m.s of concentration

Results of mean and root-mean-square (r.m.s.) profiles of concentration fluctuations (c) for different s_z have been discussed comprehensively in our recent study, Talluru *et al.* (2017). It is observed that both the normalised mean and r.m.s profiles of concentration for most source heights are well described by a reflected-Gaussian model;

$$C(z) = A\left[\exp\left\{-B\left(\frac{z-s_z}{\delta_z}\right)^2\right\} + \exp\left\{-B\left(\frac{z+s_z}{\delta_z}\right)^2\right\},\right] \quad (1)$$

where A, B and δ_z are parameters obtained by fitting the data to the equation. Figure 3 shows the normalised distributions of mean concentration (C) for all the sources as a function of local coordinate system defined about s_z as $\xi = (z-s_z)/\delta_z$. For sources located in the outer region of the boundary layer ($s_z \geq 0.5\delta$), there is a marginal deviation from reflected-Gaussian model. Overall, the mean statistics of concentration agreed well with previous studies of Fackrell & Robins (1982); Nironi *et al.* (2015) and with that validation, the analysis is being extended here to understand the interactions between velocity and concentration fluctuations.

3 AUTOCORRELATION

The spatial and temporal information of velocity and concentration fluctuations can be understood using the autocorrelation function defined as,

$$R_{ii} = \frac{\overline{i(t)i(t+\Delta t)}}{\sigma_i{}^2} \quad i = u, c \quad (2)$$

where R_{ii} is the normalised correlation coefficient. Figures 4(a) and 4(b) show autocorrelation functions of u and c respectively, calculated at the centreline of the plume for different source heights. Although a trend with varying s_z is not clear for either of R_{uu} or R_{cc} in figure 4, it is clear that time-scale over which concentration fluctuations are correlated with each other are smaller than that for velocity fluctuations. This in-turn implies that the lengths scales associated with concentration will also be smaller than length scales of the turbulent motions. This is consistent with the argument put forth by Tennekes & Lumley (1972), i.e., the interaction of turbulent and molecular transport results in much faster spread of a scalar, in other words, shorter time and length scales. In the Eulerian frame of reference, integral length scale for velocity fluctuations in a fully-

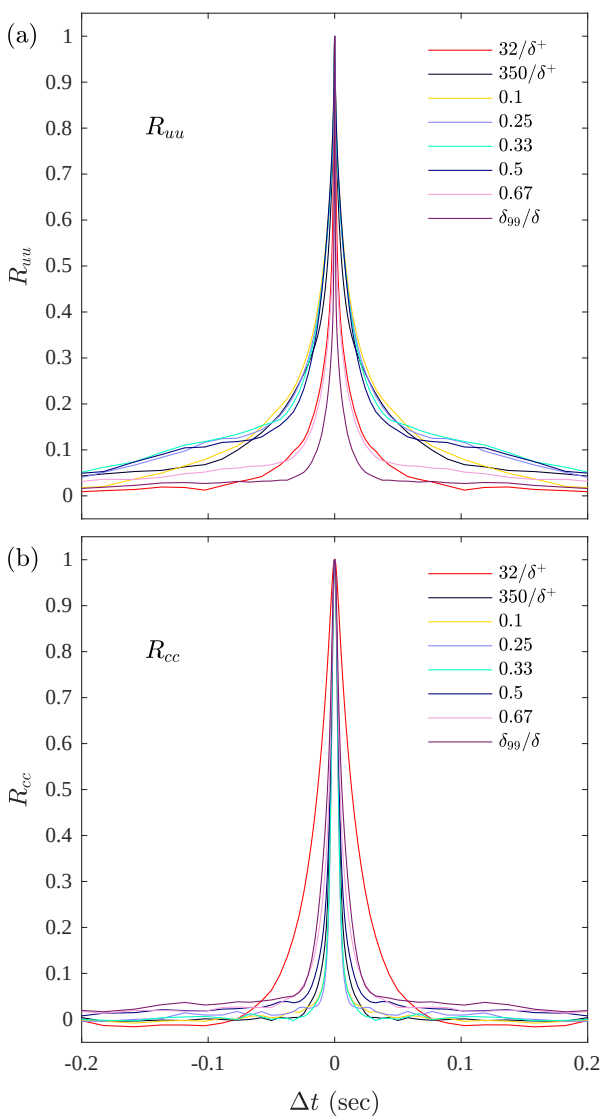

Figure 4: Autocorrelation functions of (a) velocity (R_{uu}) and (b) concentration (R_{cc}) on the centre line of the plume for different source heights.

developed turbulent flow is computed from integral time scale by invoking Taylor's frozen turbulence hypothesis and assuming local mean velocity as the convection velocity. This has been shown to be approximately valid (Dennis & Nickels, 2008; Del Álamo & Jiménez, 2009) for velocity structures in wall-bounded flows, however, this hypothesis is not applicable to scalar concentration field that is rapidly developing downstream of a point source. Hence, the discussion here is limited for the integral time scales of u and c that are unambiguously calculated from single-point measurements.

The integral time scales for velocity and concentration are denoted as τ_u and τ_c, respectively. The integral time scale (τ_i) for any fluctuating quantity (i) is defined as,

$$\tau_i = \int_0^\infty R_{ii}(t)\, dt, \quad (3)$$

and is indicative of average duration of a velocity structure or a high scalar-concentration region. The calculation of τ_i is simplified by integrating over the time duration up to first zero crossing of R_{ii}. Figures 5(a) and 5(b) plot integral time-scales for velocity and concentration, respectively, calculated at the centreline of the plume at different source heights. Note that there are 240 measurement points (30 points per source height experiment) and the scatter in the data is acceptable. Here we will only make observations of the over-

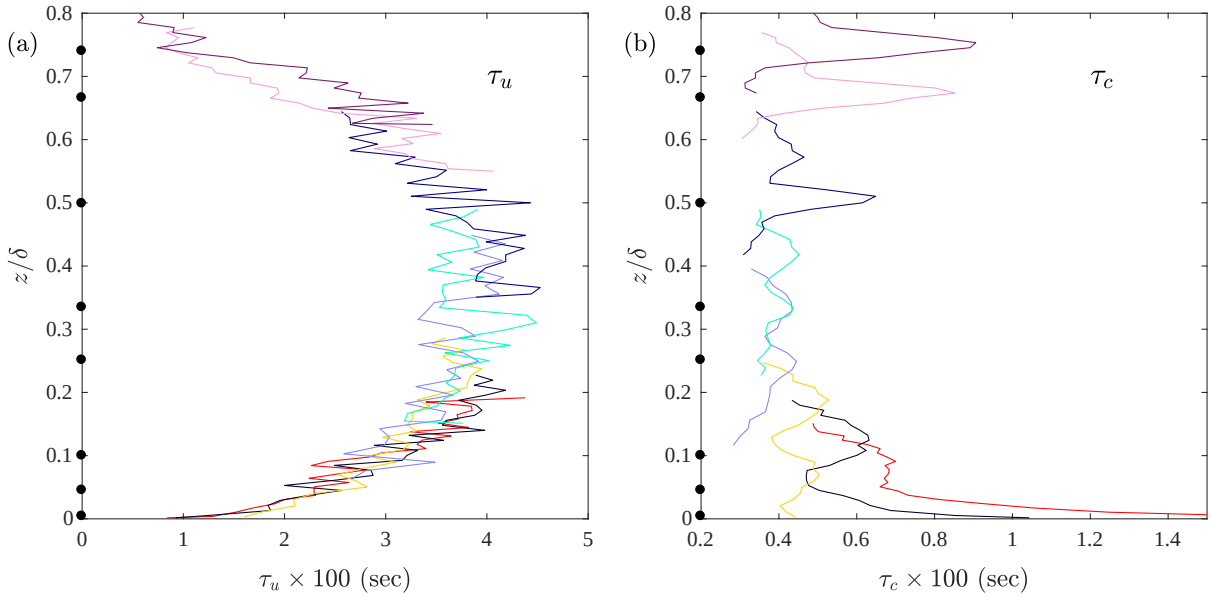

Figure 5: Comparison of integral time scales of (a) velocity and (b) concentration fluctuations for different source heights (indicated by black dots). Line colours as in figure 4.

all trend and magnitude. It is seen that τ_u increases up to $z/\delta = 0.2$, approximately remains constant between $0.2 \leq z/\delta \leq 0.5$ and then decreases up to the edge of boundary layer. Increasing trend of τ_u adjacent to the wall is expected as the large-scale motions become more prominent in the inner-boundary-layer as one moves away from the surface. In the outer part, $z/\delta > 0.5$, there is a decreasing trend of τ_u which is due to increasing influence of external intermittency, i.e. the largest length-scales that could be detected from point-measurements will be confined within regions of turbulent zones that preceded and followed by non-turbulent zones. On the other hand, the distribution of τ_c, shown in figure 4(b), varies for different source heights. The overall trend of *all data* in figure 4(b) is that τ_c is high close to the wall and near the edge of the boundary layer while it does not vary significantly in the region $0.1 < z/\delta < 0.5$. It is clear that τ_c is influenced by two factors; the background turbulence and the spread of the plume. On closer examination of τ_c profiles corresponding to a particular source height, it is seen that two distinct local peaks are present; the lower peak occurs approximately on the centreline of plume while the second peak occurs well above it. The peak in τ_c at the centreline is expected as this is the location where the tracer is released and thus the concentration levels detected are high in magnitude and less intermittent. Further, it can be seen that the peak magnitude of τ_c at the centreline increases with s_z. This is attributed to the increasing mean velocity (or convection velocity) and decreasing turbulence intensity with increasing distance away from the surface. Thus temporal variation of C is less intermittent but faster as one moves away from the wall. While the peak on the centreline sustains for different source heights in the boundary layer, the second peak gradually disappears as s_z increases. The secondary peak is further examined in detail in figure 6 where normalised $\tau_c/(\tau_c|_{\max})$ values are plotted against ξ . Note that in this coordinate system, $\xi = 1$ corresponds to half-width of a plume. This figure better illustrates that the secondary peak in τ_c is seen at $\xi \approx 2$, which is in vicinity of the edge of the plume, i.e. at the interface between the plume and the background flow. It is also noted that for $s_z/\delta = 0.1, 0.25$ and 0.33, the secondary peak in τ_c has equivalent magnitude as the primary peak near the centreline. The authors currently do not have a physical explanation for the occurrence of secondary peak and possible artefacts due to background concentration or data-processing are being

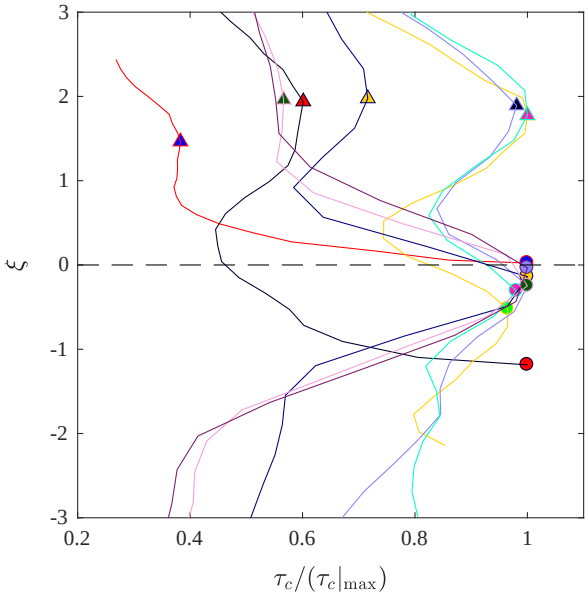

Figure 6: Normalised integral time scale of c for all source heights as a function of $\xi = (z - s_z)/\delta_z$. The peak in τ_c closer to $\xi = 0$ is shown by solid circles while the other peak is represented by solid triangles.

investigated.

On comparing τ_u and τ_c in figure 4, it is observed that quantitatively integral time-scale for velocity fluctuations is an order of magnitude larger than integral time scale for concentration, i.e. $\tau_u/\tau_c = O(10)$. This result has implications for CFD methods, especially large eddy simulation (LES), that discretize the transport equation and indicate that the grid or time-marching requirements to resolve variations in C are more stringent than those for resolving turbulent motions. The interaction between the background turbulence and concentration fluctuations is further examined by cross-correlation analysis between u and c.

4 CROSS-CORRELATION

Before computing cross-correlation functions of velocity and concentration, it is important to quantify the time lag between ve-

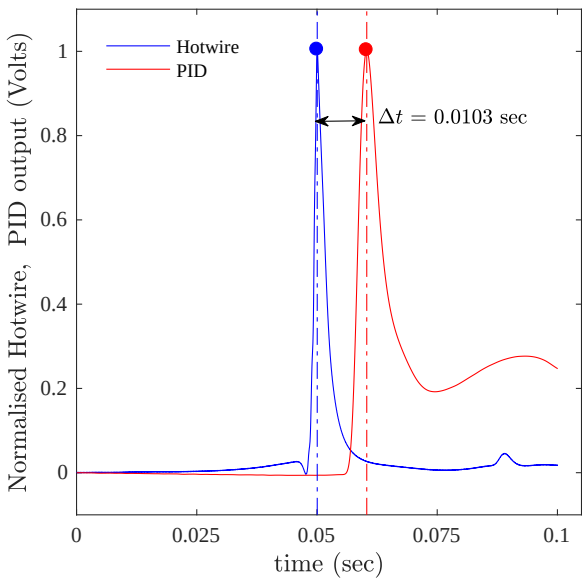

Figure 7: Time lag between hotwire and PID sensors.

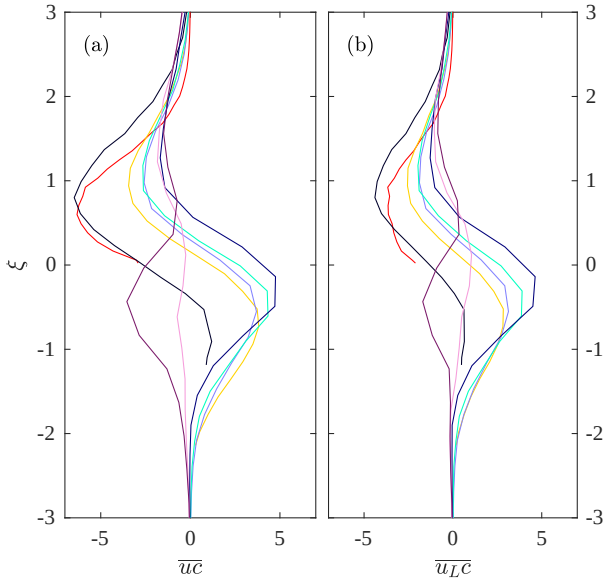

Figure 8: Comparison of (a) streamwise concentration flux ($\overline{uc}$) for different source heights and (b) the contribution of large-scales of velocity to scalar flux. Note that line colours in (a) and (b) are specified in figure 4.

locity and concentration signals. The time lag is due to delay in the response of PID sensor compared to hotwire. For this, a custom test rig is built to determine the frequency response and time lag of the PID sensor. The time lag is the time required for a gas sample to travel from the sensor tip to the detection chamber of PID. The rig consists of a rotating chopper wheel that delivers a quasi-impulse of tracer gas to the stationary PID sensor. A single hotwire probe with a frequency response of 10 kHz is placed next to the PID sensor and both sensors are sampled simultaneously to record the passage of a puff of tracer gas. Figure 7 plots the ensemble-averaged signals of 180 realisations of hotwire and PID voltages. Prior to averaging, the DC offset voltage and gain in the signals are adjusted so that the baseline and peak corresponded to 0 and 1 V respectively. It is found that the frequency response of PID is dependent on the suction flow rate; 280 Hz at the low setting, 330 Hz at a medium suction rate and increasing to 400 Hz at the high setting. The time lag is calculated as the time between the peaks in the hotwire and PID signals and is found to be 103 milli-seconds on average at the highest suction rate. In all the cross-correlation results presented below, the time lag is accordingly adjusted for concentration signals.

We first consider the wall-normal distribution of streamwise concentration flux $\overline{uc}$ in figure 8(a) for all source heights. Results are presented using the local ordinate ξ in order to examine characteristic behaviour of $\overline{uc}$ about the centreline of the plume. For source at $s_z/\delta \leq 0.5$, $\overline{uc}$ is positive below $\xi = 0$ and negative above the plume centreline, however, there is a reversal of this trend when $s_z/\delta = 0.67$ and $s_z/\delta = \delta_{99}/\delta$. The behaviour of $\overline{uc}$ below $s_z/\delta = 0.67$ can be explained by considering Reynolds shear stress term $\overline{uw}$, where w is the velocity fluctuations in the vertical direction. Positive w-fluctuations above $\xi = 0$ and the negative w-fluctuations below $\xi = 0$ contribute to vertical spread of scalar plume. It is also well-known that $\overline{uw}$ is negative across the boundary layer implying that negative u-fluctuations will correlate with positive w-fluctuations that transport C above the centreline and likewise positive u-fluctuations will correlate with transport of C by negative w-fluctuations below the centreline. Therefore, the magnitude of $\overline{uc}$ is positive below $\xi = 0$ and is negative above it. Further detailed investigation is needed to understand the trend of $\overline{uc}$ for $s_z/\delta = 0.67$ and $s_z/\delta = \delta_{99}/\delta$ by simultaneous measurements of all three components of velocity and concentration as the external intermittency and entrainment at the turbulent/non-turbulent interface will also influence the transport of C in this region.

In order to understand the contribution of large-scales of velocity to scalar flux, the instantaneous velocity is decomposed into large- and small-scales by a cut-off filter corresponding to wavelength of 1δ such that $u = u_L + u_S$, where u_L and u_S are the large- and small-scale components, respectively. The choice of 1δ as the filter cut-off is consistent with the previous studies of Hutchins & Marusic (2007*b*); Mathis *et al.* (2009) who established this threshold based on the criteria of separating inner and outer peaks in spectral distribution of velocity fluctuations. The contribution of large-scales to scalar flux $\overline{u_L c}$ is shown in figure 8(b), noting that $\overline{uc} = \overline{u_L c} + \overline{u_S c}$. It is found that $\overline{u_L c}$ contributes significantly to the magnitude of $\overline{uc}$, a result that is expected as significant portion of the streamwise turbulent kinetic energy ($\overline{uu}$) is due to the large-scale scale component u_L. However, high $\overline{u_L c}$ correlation also implies that transport of C that is well-correlated with u_L will be due to coherent features in the flow that are associated with large-scale motions. Few such large-scales motions that are well-identified in zero-pressure-gradient turbulent boundary layers are long meandering super-structures (see Hutchins & Marusic, 2007*a*), counter-rotating roll-modes (e.g. Hutchins & Marusic, 2007*b*) and vortex packets (e.g. Christensen & Adrian, 2001). Thus lateral and transverse shear stress events ($\overline{uv}$ and $\overline{uw}$) associated with large-scale motions will be responsible of instantaneous spread of the plume and its meandering.

The physical extent of interaction between large-scale velocity fluctuations u_L and concentration fluctuation c can be examined by cross-correlation coefficient $R_{u_L c}$ that is a function of time-delay between two signals.

$$R_{u_L c} = \frac{\overline{u_L(t)c(t+\Delta t)}}{\sigma_{u_L}\sigma_c}. \tag{4}$$

Results of $R_{u_L c}$ are presented as a contour map in figure 9 only for the source located in the log-region (i.e., $s_z/\delta = 0.1$) for brevity. Note that time shift (Δt) is used as the abscissa in figure 9 since the convection speed of scalar in a TBL is not known. As expected based on observations made in figure 8, large-scales of velocity are positively correlated with c below $\xi = 0$ and they are negatively correlated above the plume centreline. Further, there is clear asym-

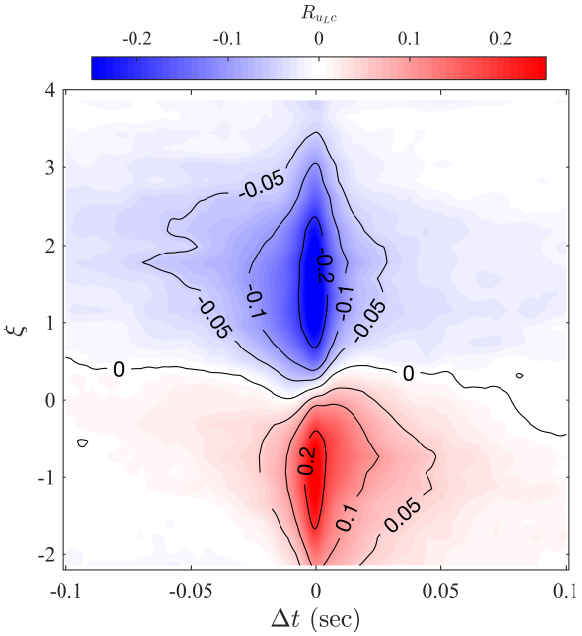

Figure 9: Two-dimensional contour map of cross-correlation (R_{u_Lc}) between large-scale component of velocity (u_L) and concentration (c) fluctuations for $s_z/\delta = 0.1$.

metry in R_{u_Lc} on either side of $\Delta t = 0$; the contours of positive correlation spread further in the positive Δt direction below $\xi = 0$ while the negative correlation above $\xi = 0$ extends more along the negative Δt direction. This implies that below the source height, large-scale high-speed turbulent fluctuations are better correlated with the concentration fluctuations upstream than those in the downstream region. Similarly, above the source height, large-scale low-speed turbulent fluctuations are better correlated with concentration fluctuations downstream than those in the upstream region. The characteristic streamwise gradient in the concentration field and the wall-normal gradient of streamwise velocity are believed to contribute to this behaviour and require further investigation using tools such as conditional analysis that is beyond the present discussion. However, it is clear that the correlation between u_L and c drops quickly within a time shift that corresponds to a physical distance of approximately 0.5δ, *if* one assumes the mean velocity at the plume centreline as the convection velocity. Thus, with observations made in figure 4, it could be inferred that the high-concentration events are significantly smaller than large-scale turbulent motions but they correlate well over extents of $O(0.5\delta)$; therefore large-scale coherent features are crucial towards understanding the mechanism of transport of scalar-fluctuations.

5 CONCLUSIONS

Simultaneous temporal measurements of velocity and concentration fluctuations have been successfully performed when a passive scalar is released from a point source at eight different heights in a turbulent boundary layer. It is found that the integral time scale of c, obtained from its autocorrelation function, is approximately ten times smaller than the integral time scale of u. Thus length-scales associated with turbulent transport of scalar will be equivalently smaller too. Measurements that can directly establish the length-scale associated with turbulent transport are imperative. Further analysis showed that high-speed and low-speed velocity fluctuations contribute to the scalar flux in different regions relative to the source height. The contribution of large-scale motions to the overall scalar flux ($\overline{uc}$) has established the importance of investigating Reynolds shear stress events associated with large-scale coherence to better understand the mechanism of turbulent transport.

REFERENCES

Chauhan, K. A., Nagib, H. M. & Monkewitz, P. A. 2009 Criteria for assessing experiments in zero pressure gradient boundary layers. *Fluid Dyn. Res.* **41**, 021404.

Christensen, K. T. & Adrian, R. J. 2001 Statistical evidence of hairpin vortex packets in wall turbulence. *Journal of Fluid Mechanics* **431**, 433–443.

Del Álamo, J. C. & Jiménez, J. 2009 Estimation of turbulent convection velocities and corrections to Taylor's approximation. *J. Fluid Mech.* **640**, 5–26.

Dennis, D. J. C. & Nickels, T. B. 2008 On the limitations of Taylor's hypothesis in constructing long structures in a turbulent boundary layer. *J. Fluid Mech.* **614**, 197–206.

Fackrell, J. E. & Robins, A. G. 1982 Concentration fluctuations and fluxes in plumes from point sources in a turbulent boundary layer. *J. Fluid Mech* **117** (1), 26.

Gailis, R. M. & Hill, A. 2006 A wind-tunnel simulation of plume dispersion within a large array of obstacles. *Bound.-Layer Meteor.* **119** (1), 289–338.

Harun, Z., Monty, J. P., Mathis, R. & Marusic, I. 2013 Pressure gradient effects on the large-scale structure of turbulent boundary layers. *J. Fluid Mech.* **715**, 477–498.

Hutchins, N. & Marusic, I. 2007*a* Evidence of very long meandering features in the logarithmic region of turbulent boundary layers. *J. Fluid Mech.* **579**, 1–28.

Hutchins, N. & Marusic, I. 2007*b* Large-scale influences in near-wall turbulence. *Phil. Trans. R. Soc. A* **365**, 647–664.

Marusic, I., Chauhan, K. A., Kulandaivelu, V. & Hutchins, N. 2015 Evolution of zero-pressure-gradient boundary layers from different tripping conditions. *J. Fluid Mech.* **783**, 379–411.

Marusic, I., McKeon, B. J., Monkewitz, P. A., Nagib, H. M., Smits, A. J. & Sreenivasan, K. R. 2010 Wall-bounded turbulent flows at high Reynolds numbers: Recent advances and key issues. *Phys. Fluids* **22** (6), 065103.

Mathis, R., Hutchins, N. & Marusic, I. 2009 Large-scale amplitude modulation of the small-scale structures in turbulent boundary layers. *J. Fluid Mech.* **628**, 311–337.

Metzger, M. M. & Klewicki, J. C. 2003 Development and characterization of a probe to measure scalar transport. *Meas. Sci. Tech.* **14** (8), 1437.

Nironi, C., Salizzoni, P., Marro, M., Mejean, P., Grosjean, N. & Soulhac, L. 2015 Dispersion of a passive scalar fluctuating plume in a turbulent boundary layer. Part I: Velocity and concentration measurements. *Bound.-Layer Meteor.* **156** (3), 415–446.

Smits, A. J., McKeon, B. J. & Marusic, I. 2011 High-Reynolds number wall turbulence. *Annu. Rev. Fluid Mech.* **43**, 353–375.

Talluru, K. M., Baidya, R., Hutchins, N. & Marusic, I. 2014*a* Amplitude modulation of all three velocity components in turbulent boundary layers. *J. Fluid Mech.* **746**, R1.

Talluru, K. M., Hernandez-Silva, C., Philip, J. & Chauhan, K. A. 2017 Measurements of scalar released from point sources in a turbulent boundary layer. *Meas. Sci. Tech.* **28** (5), 055801.

Talluru, K. M., Kulandaivelu, V., Hutchins, N. & Marusic, I. 2014*b* A calibration technique to correct sensor drift issues in hot-wire anemometry. *Meas. Sci. Tech.* **25** (10), 105304.

Tennekes, H. & Lumley, J. L. 1972 *A first course in turbulence*. MIT press.

Yee, E., Kosteniuk, P. R., Chandler, G. M., Biltoft, C. A. & Bowers, J. F. 1993 Statistical characteristics of concentration fluctuations in dispersing plumes in the atmospheric surface layer. *Bound.-Layer Meteor.* **65** (1-2), 69–109.